Multi-objective Optimal Operation of Centralized Battery Swap Charging System with Photovoltaic

Yuanzheng Li, *Member*, *IEEE*, Yihan Cai, Tianyang Zhao, *Member*, *IEEE*, Yun Liu, *Member*, *IEEE*, Jian Wang, Lei Wu, *Senior Member*, *IEEE*, and Yong Zhao

***Abstract*—Electric vehicles (EVs) are widely deployed throughout the world, and photovoltaic (PV) charging stations have emerged for satisfying the charging demands of EV users. This paper proposes a multi-objective optimal operation method for the centralized battery swap charging system (CBSCS), in order to enhance the economic efficiency while reducing its adverse effects on power grid. The proposed method involves a multi-objective optimization scheduling model, which minimizes the total operation cost and smoothes load fluctuations, simultaneously. Afterwards, we modify a recently proposed multi-objective optimization algorithm of non-sorting genetic algorithm III (NSGA-III) for solving this scheduling problem. Finally, simulation studies verify the effectiveness of the proposed multi-objective operation method.**

***Index Terms*—Multi-objective optimization, electric vehicle, battery swap charging system, scheduling, photovoltaic.**

I. Introduction

In recent years, electric vehicles (EVs) and their charging stations have been widely deployed for adapting to the clean, efficient and sustainable energy development throughout the world [1]-[3]. It is predicted by the International Energy Agency that the number of EVs will exceed 12.9 million after 2020 [4]. Indeed, the large scale of EVs may bring about great effects on the secure and stable operation of the power grid, as the huge charging demands could change the spatial and temporal distribution of loads in the power grid.

To this end, suitable charging strategies of EVs are needed to stimulate the power grid to actively provide energy services. Currently, there exist two primary schemes of EV charging, i.e., the plug-in and the battery swapping schemes [5]. Note that the latter largely improves the convenience of charging, by which EVs can obtain the energy more efficiently compared with the former [6].

Recently, researchers have carried out related studies on the battery swapping schemes. For instance, [6] proposes an optimization framework for the operation model of battery swapping stations (BSSs) based on the day-ahead scheduling. In addition, [7] introduces an optimal charging schedule of EVs in the context of BSSs. Simulation studies verify that it is helpful for decreasing the gap between the peak and valley loads, and reducing the coal consumption of traditional generators. Furthermore, a novel scheduling model for swapping EV batteries is presented in [8], which aims to minimize the operation cost of the BSS. What is more, [9] proposes a bi-level optimal scheme to promote the participation of EVs in regulating the economic operation of the power grid.

With the popularity of battery swapping in EV services, the centralized battery charging station (CBCS) has emerged. It provides charging services for depleted batteries (DBs), which then become fully-charged batteries (FCBs) and are sent to BSSs. In this way, the CBCS and BSSs constitute the centralized battery swap charging system (CBSCS), and establishing CBCSs is one of the most important areas that deserve extensive exploration [10].

Indeed, some researchers have conducted related works on the operation of CBCSs. For instance, [11] proposes a decentralized coordinated control strategy for EV fast charging station, in order to ensure the stable operation of the microgrid. Moreover, [12] shows a charging pricing strategy of EV fast charging stations, which improves the voltage profiles of distribution networks. In addition, [13] presents a two-stage stochastic optimization model to manage EV charging and reduce the costs of charging and infrastructure. Furthermore, [14] studies the optimal scheduling problem of CBCS, which is formulated as a mixed-integer program to obtain the optimal scheduling of charging processes so that the operation cost is minimized while satisfying the needs of FCBs. Similarly, [15] formulates the battery charging schedule as an inventory management problem, which aims to optimize the profit of CBCS and guarantee the demands of batteries. Moreover, as CBCS and BSSs are tightly coupled with each other via batteries, [16] proposes a battery scheduling framework, in which a two-direction battery scheduling

Manuscript received: February 26, 2020; revised: June 18, 2020; accepted: August 3, 2020. Date of CrossCheck: August 3, 2020. Date of online publication: February 17, 2021.

This work was supported by the Key Scientific and Technological Research Project of State Grid Corporation of China (No. 5400-202022113A-0-0-00).

Y. Li (corresponding author), Y. Cai, J. Wang, and Y. Zhao are with the School of Artificial Intelligence and Automation, Ministry of Education Key Laboratory of Image Processing and Intelligence Control, Huazhong University of Science and Technology, Wuhan, China (e-mail: Yuanzheng_Li@hust.edu.cn; 347530860@qq.com; wj0826_can@hust.edu.cn; zhiwei98530@hust.edu.cn).

T. Zhao is with the School of Electrical and Electronic Engineering, Nanyang Technological University, Singapore, Singapore (e-mail: zhaoty@ntu.edu.sg).

Y. Liu is with the College of Mechatronics and Control Engineering, Shenzhen University, Shenzhen, China (e-mail: liuyun19881026@gmail.com).

L. Wu is with the Department of Electrical & Computer Engineering, Stevens Institute of Technology, Hoboken, USA (e-mail: lwu11@stevens.edu).

DOI: 10.35833/MPCE.2020.000109

model is used to efficiently arrange EV batteries between the CBCS and BSSs. In addition, [17] presents a joint optimization of unit commitment and the swapping charging system of EV battery that consists of the CBCS and BSSs, in order to improve the ambient air quality and reduce the associated health impacts.

It is worthwhile to mention that, with rapid developments of renewable energies, the PV-powered CBCS has emerged in recent years [18]-[21]. In this way, considering that the CBSCS with PV integration could utilize solar energy to provide charging services for EV batteries, the operation of PV-powered CBCS and BSS has been studied, respectively. As for the PV-powered CBCS, [18] presents a PV-equipped CBCS, which provides fast EV charging services while reducing stress to power systems. Moreover, [19] proposes an autonomous energy management strategy, by which PV-assisted CBCS performs better in providing an ancillary service than the station without PV. In addition, [20] adopts a two-stage stochastic optimization method to accommodate uncertain output of PVs for CBCSs, and a Latin hypercube based sample average approximation method is used to pursue the minimum operation cost. Furthermore, [21] investigates a classification method, by which EVs in a CBCS can be divided into premium, conservative, and green ones, according to their distinct charging behaviors. It is found that green vehicles could help a PV-driven CBCS reduce its cost by using batteries as distributed storage. Similarly, to pursue the economic operation of the PV-powered BSS, [22] proposes an optimal charging scheme for BSSs with PV, which is solved by a heuristic optimization algorithm to reduce the cost. In addition, [23] presents a combined optimization method for the configuration and operation of the BSS with PV, while pursuing the economic efficiency, which also verifies the necessity of considering uncertain PV power.

Indeed, there exist some relevant works, which take the above aspects as a whole into account. In other words, they consider multiple objectives of the EV charging and PV. For instance, [24] proposes a multi-objective optimization model which aims at maximizing the revenues of the PV-based EV station and minimizing the capacity fading of battery energy storage system (BESS), simultaneously. In addition, [25] discusses the optimization scheduling problem in PV microgrid considering EV charging and demand response, which realizes the minimization of the total operation cost (TOC) and the exchange capacity with the power grid. What is more, [26] introduces a multi-objective operation of the grid-connected PV charging station, the objectives of which are set as the maximization of the renewable energy utilization ratio and the minimization of the system investment and operation costs.

Meanwhile, an optimal strategy of power control and energy management for EV charging stations using renewable energy sources is proposed in [27], which aims to reduce charging time, minimize the battery temperature during the charging process, and minimize the influence on the utility grid. Reference [28] introduces an energy exchange strategy for the PV-based BSS, with the purpose of minimizing the annual cost and maximizing the percentage of utilized PV energy. Moreover, a multi-objective optimization model for coordinated control of PV generation and EV charging is established by [29], which minimizes the fluctuation of the power transmitted to the power grid, reduces the EV charging cost, and ensures EV batteries to be fully charged.

From the relevant works mentioned above, the following issues shall be taken into account, which are the main differences of our work.

1) Considering the integration of uncertain PV power into CBSCS and the usage of batteries, it would lead to some revenues or related costs. Different from current works, we concretely model the detailed composition of TOC, i.e., the opportunity cost (OC) of PV power shortage, the opportunity revenue (OR) of PV power surplus, the scheduling cost of power purchasing (SCPP) regarding CBSCS, and the inventory cost of reserve batteries (RBs).

2) It is noted that the logistic model of batteries is important, and it has not been deeply explored, especially for the multi-objective operation of CBSCS. We have carefully studied this issue in our work. In detail, we adopt the closed loop supply chain (CLSC) [30] to model the logistic characteristic of EV batteries and realize the interaction among EV users, BSSs, and CBCS.

Therefore, the main motivation and innovation of this paper include concretely modelling the TOC of CBSCS, carefully studying the logistic model of batteries, and considering multi-objective optimal operation of CBSCS with PV integration.

In order to solve the above issues, the following aspects are studied as follows.

1) We propose a multi-objective optimization scheduling model of CBSCS with PV integration. In this way, we could study the relationship among multiple objectives, in order to provide the references for determining a proper scheduling scheme.

2) To deal with this multi-objective optimization problem, we modify a recently proposed multi-objective optimization algorithm, i.e., non-dominated sorting genetic algorithm III (NSGA-III) [31] to solve the scheduling model.

The rest of this paper is organized as follows. Section II presents the operation framework of CBSCS with PV integration. In Section III, a CLSC is introduced to describe the operation process of CBSCS. In Section IV, the formulations of our proposed multi-objective scheduling model are shown. Then, Section V introduces the modified NSGA-III and its solving procedure. In Section VI, simulation studies verify the effectiveness of the proposed scheduling model and the modified algorithm. Finally, conclusions are drawn in Section VII.

II. CBSCS WITH PV INTEGRATION

It is well-known that solar energy is clean and renewable, since no carbon emission is involved in its generation. With the development of PV technology, it is a popular trend to integrate solar energy into the power grid. Note that the CBSCS with PV integration has emerged, and the charging load of EVs can be satisfied with PV supply and external power grid. This system contains battery flow, energy flow, and in-

formation flow, as shown in Fig. 1. In the battery flow, CBCS dispatches FCBs to BSSs, which then swap them for EV users. BSS receives DBs from EV users, and sends them to CBCS for charging. Meanwhile, the energy flow involves solar energy input in CBSCS as well as electric power purchased from external power grid to battery charging services. Also, if the solar power in some time intervals is abundant, it can be sold to the power grid.

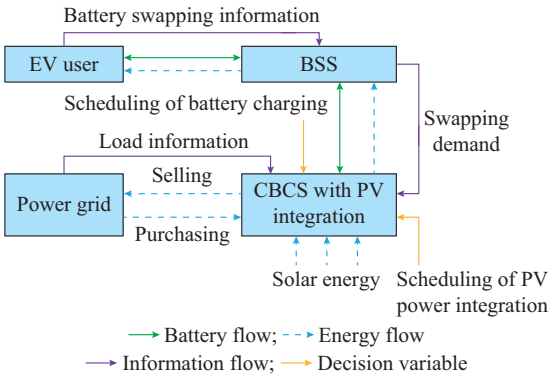

Fig. 1. Operation diagram of CBSCS with PV integration.

We need to consider PV generation uncertainties in the operation of CBSCS. In order to better understand the impact of PV power uncertainty, we establish its probability distribution, in which we assume the forecasting error follows the normal distribution, where the mean and standard deviations (SDs) are set as 0 and 8% of the forecasting power value, respectively. By applying Monte Carlo simulation [32] with the sample size of 10000, the frequency distribution of PV power can be obtained as shown in Fig. 2, where the forecasting power value is set to be 30 MW. For achieving a better operation of CBSCS, the scheduling plan of PV power input needs to be determined in advance. However, the actual power is usually deviated from the pre-determined one. Therefore, two cases will be confronted in actual dispatching, i.e., PV power shortage and surplus. In the former case, the actual PV power input is lower than the pre-determined one, which may lead to power purchasing from the power grid to CBSCS. In the latter case, the actual PV power is higher than the pre-determined one, which may result in PV power selling from CBSCS to the power grid.

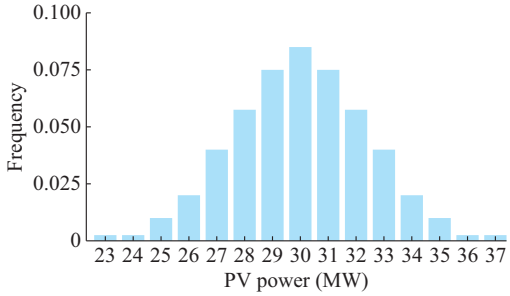

Fig. 2. Probability information of PV power.

Moreover, CBSCS receives the swapping demand and load information from BSS and the power grid, respectively. Besides, there also exists battery swapping information of EV users, which is sent to BSS via the information flow. In this way, the CBSCS also needs to determine the optimal scheduling plans of battery charging, in order to enhance the better operation of the CBSCS.

III. CLSC

To well describe the operation process of CBSCS, we use the CLSC on the basis of batteries. It is noted that the CLSC is proposed based on reverse logistics, which aims to handle the product returned, decrease the waste and provide users services at low costs [33], [34].

Generally speaking, the CLSC could be classified into four categories: C-type, M-type, R-type, and 3P-type [30]. In the C-type of CLSC, the BSS and CBCS belong to the same system, in which the products are dispatched by BSS. Meanwhile, in M-type, R-type, and 3P-type of CLSC, the BSS and CBCS belong to different systems, and the products are delivered by CBCS, BSS, and the third-party firm, respectively. It is worth mentioning that the retail price of products in the C-type is lower than those in other types [30].

Regarding EVs with battery swapping mode, it means that the price of replacing batteries is lower, which is beneficial for the development of EVs. In addition, the BSS and CBCS in the same system could share the information, in order to enhance the operation feasibility of the system. Hence, we adopt the C-type of CLSC in this paper, as shown in Fig. 3. Note that the CLSC consists of the forward supply chain (FSC), which provides products for users. It also includes the reverse supply chain (RSC), in order to callback the products used. In detail, BSS in CLSC is taken as the retailer, which provides FCBs for EV users and recycles DBs from them. In order to satisfy the swapping demand of BSS, the CBCS in the CLSC serves as the manufacturer, which provides charging services for DBs and dispatches FCBs and RBs to BSS. What is more, the energy utilized in charging module of CBCS stems from the electricity from external power grid and the solar energy.

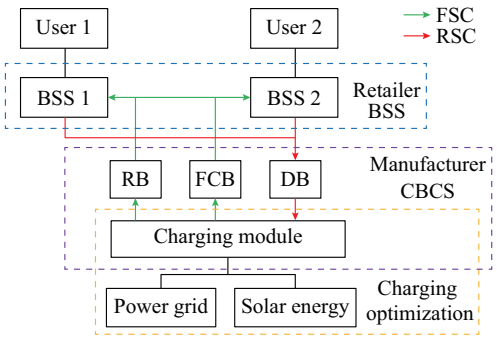

Fig. 3. Operation process of CBSCS based on CLSC.

A. Operation of Electric Bus and Taxi

Considering the battery swapping demand of users, due to the large-scale development of EVs and the diversity of objective conditions, this paper focuses on electric buses and taxies as users. Regarding the bus dispatching, we assume that buses are departed at equal intervals for convenience [35], and we divide buses into two queues and then dispatch

them alternately. In other words, we dispatch one queue in normal time and switch to the other queue when the state of charge (SOC) of all buses in the current queue is lower than the threshold value of SOC. Note that at peak time, we dispatch two queues at the same time.

In this paper, buses are departed in order, as shown in Fig. 4. Figure 4 lists the dispatching sequence of individual time slots, where T_{on} is the starting time of operation; $T_{peak,on}$ and $T_{peak,off}$ are the starting and ending time of peak time, respectively, taking the morning peak as an example; and T_a, T_b, and T_c are the next departure time after $T_{peak,off}$, the time when all buses in the current queue need to be charged, and the next departure time after T_b, respectively. It is worth noting that the first bus departed is the bus No. $(j+1)$, rather than the bus No. 1, when the other queue starts to be dispatched in normal time.

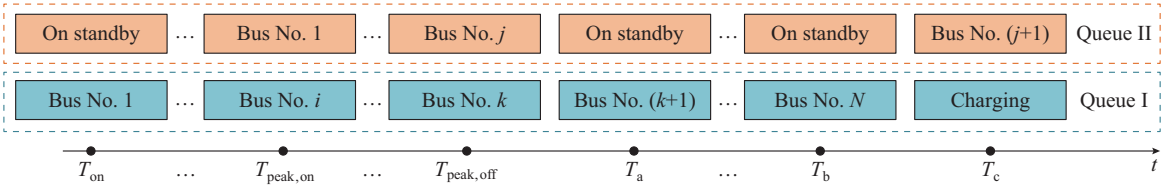

Fig. 4. Operation process of CBSCS based on CLSC.

Meanwhile, based on the research on taxi operation [36], we assume that the daily mileage of taxies is 350-500 km and there are two shifts per taxi alternating every 24 hours and 12 hours, respectively. In the two situations, the number of taxies and the off-the-line characteristic are different. The battery swapping time and SOC are shown in Table I.

TABLE I
BATTERY SWAPPING TIME AND SOC OF ELECTRIC TAXIES

Type	Battery swapping time	SOC
Alternate every 24 hours	$\mathcal{U}$(02:00,05:00) and $\mathcal{U}$(11:30,14:30)	$\mathcal{N}$(0.30,0.33)
Alternate every 12 hours	$\mathcal{U}$(02:00,04:00) and $\mathcal{U}$(11:30,14:00)	$\mathcal{N}$(0.30,0.33)

Note: $\mathcal{U}$ represents the uniform distribution; and $\mathcal{N}$ represents the normal distribution.

B. Scheduling Batteries Between BSS and CBCS

Considering the scheduling of BSS and CBCS, the replaced ones should be classified and processed to control them effectively since batteries in CBSCS are numerous. Meanwhile, their charging characteristics provide a basis for classification.

The charging mode for EV batteries can be selected as the two-stage charging mode [37]. In the first stage, batteries are charged in the constant-current mode, while they are charged via the constant-voltage mode in the second stage. The advantage of the method is that it can guarantee both the charging speed and the security in the charging process for batteries. The chargers offer charging services for batteries, and the rated power of each charger is a constant [38].

Considering that there is no interruption in the charging process and the charging time of batteries with different SOC values is different, we can divide batteries into N categories, as shown in (1), based on SOCs in the battery swapping process and their charging characteristics.

$$N=\left\lceil \frac{\max\limits_{i\in B}\left(SOC_i\right)-\min\limits_{i\in B}\left(SOC_i\right)}{p_c\eta_c\Delta h}C_r \right\rceil \tag{1}$$

where B, SOC_i, and p_c are the set of batteries in swapping time, SOC of the i^{th} battery, and the rated charging power of the charger, respectively; η_c is the charging efficiency; Δh is set as 1 hour; C_r is the rated energy of the battery; and $\lceil x \rceil$ is the smallest integer number that is not smaller than x, i.e., the ceiling function.

The battery charging time of the k^{th} category $T_{c,k}$ could be formulated as:

$$T_{c,k}=\left(k_0+k-1\right)\Delta h \tag{2}$$

$$k_0=\left\lfloor \frac{SOC_{ub}-\max\limits_{i\in B}\left(SOC_i\right)}{p_c\eta_c\Delta h}C_r \right\rfloor \tag{3}$$

where k_0 is the minimum battery charging time in the set B; SOC_{ub} is the upper boundary of SOC; and $\lfloor x \rfloor$ is the biggest integer number that is not bigger than x, i.e., the floor function.

In addition, the relationship of batteries and the corresponding category could be shown as follows.

$$I_{i,k}=\begin{cases}1 & k_0-1+k\le \dfrac{SOC_{ub}-SOC_i}{p_c\eta_c\Delta h}C_r<k_0+k\\ 0 & \text{otherwise}\end{cases} \tag{4}$$

where $I_{i,k}$ is a binary variable, if it is 1, it means battery i belongs to the k^{th} category.

Moreover, we consider that batteries are merely dispatched at several fixed moments to reduce the delivery times, and adopt the equal interval dispatching mode. Therefore, we define the dispatching time set S_d as $\{1, 1+\Delta T, \ldots, T-\Delta T+1\}$, where ΔT is the dispatching time interval; and T is the total dispatching time, which is 24 hours in this paper. Meanwhile, we use Δt and $T_{c,k}$ to denote the dispatching step and the charging time of batteries in the class k $(k=1,2,\ldots,N)$, respectively. Hence, ΔT satisfies (5), which means T can be divided evenly by ΔT.

$$\mathrm{mod}\left(T,\Delta T\right)=0 \tag{5}$$

The number of batteries in the k^{th} category which need to be dispatched from the BSS to CBCS at time t, denoted as $Q^t_{Db,k}$, is equal to the total amount of batteries swapped in the time interval $[t-\Delta T, t)$, which is formulated as:

$$Q^t_{Db,k}=\sum_{j=t-\Delta T}^{t}Q^j_{D,k}=\sum_{j=t-\Delta T}^{t}\sum_{i=1}^{Q^j_b}I^j_{i,k}\quad t\in S_d \tag{6}$$

$$Q_{\mathrm{D}}^{t}=\sum_{k=1}^{N}Q_{\mathrm{D},k}^{t} \tag{7}$$

where $Q_{\mathrm{D},k}^{j}$ and $Q_{\mathrm{D},k}^{t}$ are the numbers of batteries swapped by EV users in class k at time j and t, respectively; and Q_{D}^{j} and Q_{D}^{t} are the total numbers of batteries swapped by EV users at time j and t, respectively.

As shown Fig. 5, the batteries swapped by EV users at time $t_0-\Delta T$ are delivered to CBCS at time t_0. Analogously, the DBs swapped at time t_0 and $t_0+\Delta T$ are dispatched to CBCS at time $t_0+\Delta T$ and $t_0+2\Delta T$, respectively.

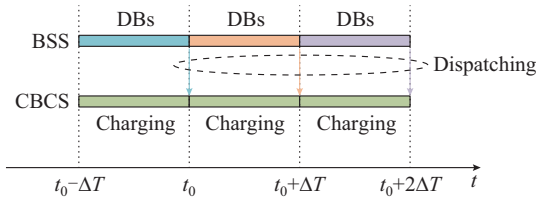

Fig. 5. Dispatching of DBs from BSS to CBCS.

The number of batteries Q_{Dc}^{t} that CBCS dispatches to the BSS at time t can be derived as the sum of batteries demanded in the time interval $[t, t+\Delta T)$, which is formulated as:

$$Q_{\mathrm{Dc}}^{t}=\sum_{k=1}^{N}Q_{\mathrm{Dc},k}^{t}=\sum_{k=1}^{N}\sum_{j=t}^{t+\Delta T}Q_{\mathrm{D},k}^{j}=\sum_{k=1}^{N}\sum_{j=t}^{t+\Delta T}\sum_{i=1}^{Q_{\mathrm{D}}^{j}}I_{i,k}^{j}\quad t\in S_d \tag{8}$$

where $Q_{\mathrm{Dc},k}^{t}$ is the number of batteries delivered from the CBCS to BSS in class k at time t.

IV. Multi-objective Optimization Scheduling Model of CBSCS

The decision variables of CBSCS consist of the scheduling plans of PV power input and battery charging, which are based on the day-ahead scheduling. Concretely speaking, since we classify the batteries into two categories and set the total dispatching time as 24 hours, there exist 48 decision variables representing the number of batteries in each category charged in each time interval and 24 decision variables denoting the predetermined PV power input value in each time interval. In addition, the PV power input plan is related to the uncertainty of solar radiation, while the battery charging plan is associated with the battery swapping behavior of EV users. Note that there exists the situation that the scheduling plan of PV power input cannot satisfy the battery charging. Hence, we need to determine the day-ahead plan of power purchasing. Meanwhile, from Section II, it can be observed that the actual PV power usually deviates from our day-ahead scheduling plan of PV power input. Therefore, there exist two cases, i.e., PV power shortage and surplus. The former situation leads to the power purchasing cost. On the contrary, in the latter situation, we could sell the surplus PV power, which contributes to the power selling revenue. In this way, we define the SCPP, the OC of PV power shortage, and the OR of PV power surplus, respectively. Also, RBs existing in the CBSCS should satisfy the swapping demand of EV users, which brings about the inventory cost. Therefore, the operation cost of CBSCS consists of these four parts.

It has been indicated that disordered or uncontrolled charging of EVs leads to load fluctuations of the power grid, i.e., expanding the load peak-valley difference, which will threaten the secure operation. Therefore, the orderly/coordinated charging has been proposed to shift the peak power demands to off-peak hours [8], [39]. The key idea of orderly/coordinated charging is based on the load shifting strategy, which considers the effect of charging load at the power grid side. In this way, the EV aggregator could allocate the charging load in different time intervals, in order to realize the peak-shaving and valley-filling [40], [41]. In this way, we also include the smoothing of the total loads as another objective in our work. Consequently, we consider both the operation cost of CBSCS and smoothing the load fluctuation by orderly charging as multiple objectives. The formulations of these objectives and corresponding constraints are presented in Section IV-A to Section IV-C. Besides, we adopt the Pareto front to present the solutions derived from our multi-objective optimization scheduling model. Therefore, the introduction of Pareto front is shown in Section IV-D.

A. Minimizing TOC of CBSCS

Note that the TOC consists of four parts, i.e., the OC of PV power shortage, the OR of PV power surplus, the SCPP and the inventory cost of RBs. The detailed description is presented as follows.

1) OC of PV Power Shortage

The OC of PV power shortage is defined as the cost of purchasing electric power from external power grid when the actual PV power input is lower than the pre-determined one. In order to model this cost, we need to take three factors into account: ① the probability when PV power shortage occurs; ② the difference between actual power output and the pre-determined one; and ③ the purchasing price of electric power. Then, the OC of PV power shortage C_{L} is formulated as:

$$C_{\mathrm{L}}^{t}=K_{\mathrm{L}}\Pr\left(P_{\mathrm{pv}}^{t}<P_{\mathrm{schedule}}^{t}\right)\left(P_{\mathrm{schedule}}^{t}-E_{P_{\mathrm{pv}}^{t}<P_{\mathrm{schedule}}^{t}}\left(P_{\mathrm{pv}}^{t}\right)\right) \tag{9}$$

$$C_{\mathrm{L}}=\sum_{t=1}^{T}C_{\mathrm{L}}^{t} \tag{10}$$

where $P_{\mathrm{schedule}}^{t}$ and P_{pv}^{t} are the pre-determined PV integration plan and the actual PV power at time t, respectively; $\Pr\left(P_{\mathrm{pv}}^{t}<P_{\mathrm{schedule}}^{t}\right)$ and $E_{P_{\mathrm{pv}}^{t}<P_{\mathrm{schedule}}^{t}}\left(P_{\mathrm{pv}}^{t}\right)$ are the probability of PV power shortage and the expected PV power when $P_{\mathrm{pv}}^{t}<P_{\mathrm{schedule}}^{t}$, respectively; C_{L}^{t} is the PV power shortage at time t; and K_{L} is the purchasing price of electric power.

2) OR of PV Power Surplus

The OR of PV power surplus is defined as the revenue of selling surplus PV power to external power grid, when the actual PV power input is higher than the pre-determined one. For modelling this revenue, we also take three factors into account: ① the probability when PV power surplus occurs; ② the difference between actual power output and the pre-determined one; and ③ the selling price of surplus PV power to external power grid. Therefore, the OR of PV power surplus R_{H} can be formulated as:

$$R_{\mathrm{H}}^{t}=K_{\mathrm{H}}\Pr\left(P_{\mathrm{pv}}^{t}>P_{\mathrm{schedule}}^{t}\right)\left(E_{P_{\mathrm{pv}}^{t}>P_{\mathrm{schedule}}^{t}}\left(P_{\mathrm{pv}}^{t}\right)-P_{\mathrm{schedule}}^{t}\right) \quad (11)$$

$$R_{\mathrm{H}}=\sum_{t=1}^{T}R_{\mathrm{H}}^{t} \quad (12)$$

where $\Pr\left(P_{\mathrm{pv}}^{t}>P_{\mathrm{schedule}}^{t}\right)$ and $E_{P_{\mathrm{pv}}^{t}>P_{\mathrm{schedule}}^{t}}\left(P_{\mathrm{pv}}^{t}\right)$ are the probability of PV power surplus and the expected PV power input when $P_{\mathrm{pv}}^{t}>P_{\mathrm{schedule}}^{t}$, respectively; R_{H}^{t} is the OR of PV power surplus at time t; and K_{H} is the price of surplus PV power selling to the power grid.

3) SCPP

SCPP is defined as the day-ahead cost we should pay, in case our scheduling plan of PV power input cannot satisfy the needs corresponding to our battery charging plan. Therefore, the SCPP C_{S} can be formulated as:

$$C_{\mathrm{S}}^{t}=\begin{cases}K_{\mathrm{L}}\left(P_{\mathrm{c}}^{t}-P_{\mathrm{schedule}}^{t}\right) & P_{\mathrm{c}}^{t}>P_{\mathrm{schedule}}^{t},\forall t\in[1,T]\\ 0 & \text{otherwise}\end{cases} \quad (13)$$

$$C_{\mathrm{S}}=\sum_{t=1}^{T}C_{\mathrm{S}}^{t} \quad (14)$$

where C_{S}^{t} is the SCPP at time t; and P_{c}^{t} is the charging load in CBCS at time t, which is formulated as:

$$P_{\mathrm{c}}^{t}=\frac{Q_{\mathrm{c}}^{t}p_{\mathrm{c}}}{1000}\quad \forall t\in[1,T] \quad (15)$$

where Q_{c}^{t} is the quantity of batteries in charging at time t.

4) Inventory Cost of RBs

As for the operation of CBSCS, it is evident that the quantity of RBs will lead to the inventory cost. For convenience, we consider the price coefficient of RBs K_{R} as constant. Hence, the inventory cost of RBs C_{R} can be formulated as:

$$C_{\mathrm{R}}=K_{\mathrm{R}}Q_{\mathrm{r}} \quad (16)$$

where Q_{r} is the number of RBs, which is shown as follows.

$$Q_{\mathrm{r}}=\sum_{t=1}^{T}Q_{\mathrm{r}}^{t}=\sum_{t=1}^{T}\max\left(Q_{\mathrm{Dc}}^{t}-Q_{\mathrm{cd}}^{t},0\right) \quad (17)$$

where Q_{cd}^{t} is the battery that has completed the charging at time t; and Q_{r}^{t} is the number of RBs at time t.

Therefore, the TOC of CBSCS C_{total} can be formulated as:

$$\begin{aligned}C_{\mathrm{total}}=C_{\mathrm{L}}-R_{\mathrm{H}}+C_{\mathrm{S}}+C_{\mathrm{R}}=&K_{\mathrm{L}}\Pr\left(P_{\mathrm{pv}}^{t}<P_{\mathrm{schedule}}^{t}\right)\cdot\\&\left(P_{\mathrm{schedule}}^{t}-E_{P_{\mathrm{pv}}^{t}<P_{\mathrm{schedule}}^{t}}\left(P_{\mathrm{pv}}^{t}\right)\right)-K_{\mathrm{H}}\Pr\left(P_{\mathrm{pv}}^{t}>P_{\mathrm{schedule}}^{t}\right)\cdot\\&\left(E_{P_{\mathrm{pv}}^{t}>P_{\mathrm{schedule}}^{t}}\left(P_{\mathrm{pv}}^{t}\right)-P_{\mathrm{schedule}}^{t}\right)+\sum_{t=1}^{T}C_{\mathrm{S}}^{t}+K_{\mathrm{R}}Q_{\mathrm{r}}\end{aligned} \quad (18)$$

B. Smoothing Load Fluctuation

It is noted that the CBSCS is usually connected to the power grid. Evidently, the charging process will influence the load fluctuation, the decrease of which can effectively reduce the line loss, optimize the load characteristic, and improve the facility utilization [42], etc. Therefore, we optimize the battery input schedule to decrease the load SD for weakening the adverse effect of charging process. The load SD is formulated as:

$$\min P_{\mathrm{var}}=\frac{1}{T-1}\sqrt{\sum_{t=1}^{T}\left[P_{\mathrm{local}}^{t}+P_{\mathrm{c}}^{t}-\sum_{i=1}^{T}\left(P_{\mathrm{local}}^{i}+P_{\mathrm{c}}^{i}\right)\Big/T\right]^{2}} \quad (19)$$

where P_{local}^{t} is the non-charging load in the converting station at time t.

C. Constraints

1) Charging Facility Constraint

In CBSCS, limited by the number of chargers N_{OI}, Q_{c}^{t} should satisfy:

$$Q_{\mathrm{c}}^{t}\le N_{\mathrm{OI}}\quad \forall t\in[1,T] \quad (20)$$

2) Constraint on Batteries to be Charged

The number of batteries planned to be charged $Q_{\mathrm{in},k}^{t}$ is no more than the amount of DBs in the CBCS at time t $Q_{\mathrm{de},k}^{t}$.

$$0\le Q_{\mathrm{in},k}^{t}\le Q_{\mathrm{de},k}^{t}\quad \forall t\in\left[1,T-T_{\mathrm{c},k}\right],\forall k\in[1,N] \quad (21)$$

3) Charging Mission Constraint

To complete the charging, the number of FCBs $Q_{\mathrm{fc},k}^{t}$ should be equal to the amount of DBs.

$$\sum_{t=1}^{T}Q_{\mathrm{fc},k}^{t}=\sum_{t=1}^{T}Q_{\mathrm{de},k}^{t}\quad \forall k\in[1,N] \quad (22)$$

4) Demand Constraint

In order to satisfy the battery swapping demand of users, the quantity of available batteries in CBSCS should be not less than the swapping demand.

$$Q_{\mathrm{fc}}^{t}+Q_{\mathrm{r}}^{t}\ge Q_{\mathrm{Dc}}^{t}\quad \forall t\in S_{d} \quad (23)$$

5) Peak Load Constraint

The charging load of the CBSCS will increase the total load demand of the power grid, which should be limited due to the peak load constraint.

$$P_{\mathrm{c}}^{t}+P_{\mathrm{local}}^{t}\le(1+\beta)\max\left(P_{\mathrm{local}}^{t}\right)\quad \forall t\in[1,T] \quad (24)$$

where P_{local}^{t} is the charging load of the local demand of the power grid at time t; and β is load increase coefficient, which is set to be 0.2 in this paper.

6) Minimum Dispatching Time Interval

From (3), we can observe that the battery swapped in the last dispatching interval $[t-\Delta T,t)$ is dispatched from BSS to CBCS, and the charging time allowed is in the time interval $[1,T-T_{c,k}]$. Therefore, in order to complete the charging mission, we should make sure that the batteries with the longest charging time can be completely charged in the final dispatching time interval. Meanwhile, we assume that they are in class N. Then, we can obtain (25), which is equivalent to (26).

$$T-T_{\mathrm{c},N}>T-\Delta T \quad (25)$$

$$\Delta T>T_{\mathrm{c},N} \quad (26)$$

D. Pareto Front

It should be mentioned that a global optimal solution does not usually exist, by which all objective functions are simultaneously minimized in a multi-objective optimization problem [43]. Consequently, the Pareto methodology is used to obtain a set of solutions, and they are non-dominated by other feasible solutions. Non-dominated solutions are also called Pareto solutions or Pareto set, and they could manifest the trade-off among multiple objectives. The reason is that an objective cannot be further improved without degrading at least one of the other objectives, in terms of a Pareto

solution. Accordingly, the concept of Pareto front is introduced as follows [43].

In a multiple minimization problem that contains objective functions f_i $(i=1,2,\ldots,n)$, where n is the total number of objective functions, a solution $\boldsymbol{x}_1$ dominates $\boldsymbol{x}_2$ only if the following relationships are satisfied, simultaneously.

$$f_i(\boldsymbol{x}_1) \le f_i(\boldsymbol{x}_2) \quad \forall i \in 1,2,\ldots,n \tag{27}$$

$$f_i(\boldsymbol{x}_1) < f_i(\boldsymbol{x}_2) \quad \exists i \in 1,2,\ldots,n \tag{28}$$

Otherwise, $\boldsymbol{x}_1$ and $\boldsymbol{x}_2$ are non-dominated, and they comprise Pareto set. Afterwards, the Pareto optimal solutions can be selected in this set by the comparisons, i.e., no other solutions correspond to better objective values. Therefore, we obtain the objective values regarding Pareto optimal solutions, which comprise the Pareto front as shown in Fig. 6, taking two objectives as an instance. Evidently, the trade-off between different objectives is clearly shown, which could provide valuable reference for decision making.

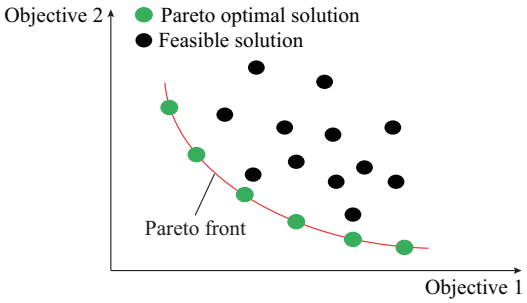

Fig. 6. Illustration of Pareto front.

V. Modified NSGA-III

The above multi-objective scheduling of the CBSCS is a high-dimension and nonlinear optimization problem, while the strong coupling between FSC and RSC further complicates its computation. Therefore, we adopt a recently proposed multi-objective optimization algorithm, i.e., NSGA-III, which could well handle such a complex, multi-objective and nonlinear optimization problem. It is noted that the rates of crossover and mutation are the key parameters for NSGA-III [31]. The crossover operator could help search better solutions, since it introduces new solutions into the population. The mutation operator is used to adjust existing solutions, in order to obtain better ones. It should be mentioned that the solutions may be disrupted faster than the selection exploiting them, when the crossover rate is higher during the final iterations. Besides, it may bring about the premature convergence of the algorithm to the suboptimal solutions if the mutation rate is higher in the initial iterations [44]. Hence, the rates of crossover and mutation need to be gradually decreased and increased with the progress of iterations, respectively. In this way, we adopt an adaptive parameter control method for tuning the rates of crossover and mutation. This is the main improvements of the modified NSGA-III.

In the following, we present the descriptions of NSGA-III and the modified version using the adaptive parameter control method.

A. NSGA-III

1) Non-dominated Sorting Genetic Algorithm II (NSGA-II)

Since NSGA-III is an enhancement of NSGA-II, first of all, we briefly introduce this original algorithm [43]. Taking the t^{th} generation as an example, we denote the parent population and the offspring population as P_t and Q_t, respectively, the sizes of which are both set as N. In order to preserve elite members, we need to select the best N members from the combined population $R_t = P_t \cup Q_t$. To realize this issue, we divide R_t into several non-domination levels, donated as $F_1, F_2, ..., F_l$. Then, starting from F_1, we accept those more optimal non-domination levels to compose the new generation S_t. Mostly, the final selected level F_l is partially accepted, via computing the crowding distance of each member. Afterwards, we choose those solutions whose crowding distances are larger, in order to enhance the evenness degree of the Pareto front.

2) Determination of Reference Point on a Hyper-plane

Unlike NSGA-II, NSGA-III adopts a number of reference points, which are placed on a normalized hyper-plane, in order to guarantee the diversity of non-dominated solutions. The hyper-plane is equally leaned to all objective axes and has an intercept of one on each axis [45], [46]. Suppose that there are p divisions along each objective, the total quantity of reference points H in an M-objective problem is formulated as:

$$H = \begin{bmatrix} M+p-1 \\ p \end{bmatrix} \tag{29}$$

where M is the number of objectives. In this paper, we study a two-objective problem, which means that $M=2$.

In addition, we stress that population members are in a sense associated with each reference point. Since these points are widely scattered on the entire hyper-plane, we can infer that the obtained solutions are also likely to be widely scattered on or close to the optimal Pareto front.

3) Adaptive Normalization of Population Member

First, we need to derive a set of ideal points of the population S_t by confirming the minimum value $z_i^{\min}$ of each objective function. Then, we translate all objective values of each individual in S_t by subtracting them from $z_i^{\min}$, so that the ideal point of translated S_t will be a zero vector. Afterwards, we confirm the extreme point in the j^{th} objective axis via deriving the solution $(\boldsymbol{x} \in S_t)$ that minimizes the following achievement scalarizing function with weight vector $\boldsymbol{w} = [w_1, w_2, \ldots, w_M]^{\mathrm{T}}$.

$$ASF(\boldsymbol{x}, \boldsymbol{w}) = \max_{i=1,2,\ldots,M} \frac{f_j'(\boldsymbol{x})}{w_i} \quad \boldsymbol{x} \in S_t, j = 1,2,\ldots,M \tag{30}$$

$$w_i = \begin{cases} 10^{-6} & i \ne j \\ 1 & i = j \end{cases} \tag{31}$$

where $f_j'(\boldsymbol{x})$ is the translating objective, i.e., $f_j'(\boldsymbol{x}) = f_j(\boldsymbol{x}) - z_j^{\min}$.

Finally, we construct a M-dimensional linear hyper-plane with these M extreme vectors and normalize objective functions as follows.

$$f_i^{\mathrm{n}}(\boldsymbol{x})=\frac{f_i(\boldsymbol{x})-z_i^{\min}}{a_i-z_i^{\min}} \quad i=1,2,\ldots,M \tag{32}$$

4) Association Operation

As mentioned above, we can associate each population member with a reference point for obtaining better solutions. In order to achieve this, a reference line corresponding to each reference point is defined by connecting the reference point with the origin. As a result, we associate each population member to the reference point, whose reference line is closest to this member.

5) Niche-preservation Operation

We first represent the niche count, which is the quantity of reference-point-associated population members from $P_{t+1}=S_t/F_l$, as ρ_j for the j^{th} reference point. Then, we obtain the $\bar{j}^{\mathrm{th}}$ reference point, which is randomly selected from the reference point set with the minimum ρ_j.

If $\rho_{\bar{j}}=0$, it means that there is no P_{t+1} member associated with the reference point $\bar{j}$, and there will be two schemes with $\bar{j}$ in Pareto front F_l. One is to select the member whose perpendicular distance from this reference line is the shortest. Afterwards, the niche count $\rho_{\bar{j}}$ has to be increased by one. Otherwise, we should remove this reference point from the current generation, since Pareto front F_l does not have any members associated with $\bar{j}$.

If $\rho_{\bar{j}}\geq 1$, meaning that there is at least one member associated with $\bar{j}$, we should randomly choose a member associated with $\bar{j}$ from front F_l, and the count $\rho_{\bar{j}}$ should be added by one. Updating niche counts, we repeat the procedure for K times until all vacant population slots of P_{t+1} is filled up.

B. Adaptive Parameter Control Method

The rates of crossover and mutation, i.e., P_{c} and P_{m}, are fixed in traditional NSGA-III, which may find unsatisfactory Pareto solutions, as discussed at the beginning of Section V. Therefore, in order to further enhance the searching performance of NSGA-III and the quality of our solution set, we decrease and increase the rates of crossover and mutation in a specific way, shown as follows, respectively.

$$P_{\mathrm{c}}=\frac{1}{\alpha+\beta\sin f} \tag{33}$$

$$P_{\mathrm{m}}=\frac{1}{\alpha+\beta\cos f} \tag{34}$$

$$f=\frac{i}{I_{\max}} \quad 1\leq i\leq I_{\max} \tag{35}$$

where $I_{\max}$ is the maximum number of iterations; and the indices α and β are set to be 1.05 and 0.15, respectively.

C. Solving Process

This subsection presents the solving process in Fig. 7. Firstly, when the information of battery swapping demands of electric buses, taxies, loads, and PV samples are obtained, we conduct the parameter initialization such as the quantity of chargers, population size, initial crossover, mutation operator, etc. Secondly, we generate reference points to construct the hyper-plane. Thirdly, the population is initialized through obtaining random values between the upper and lower bounds of decision variables.

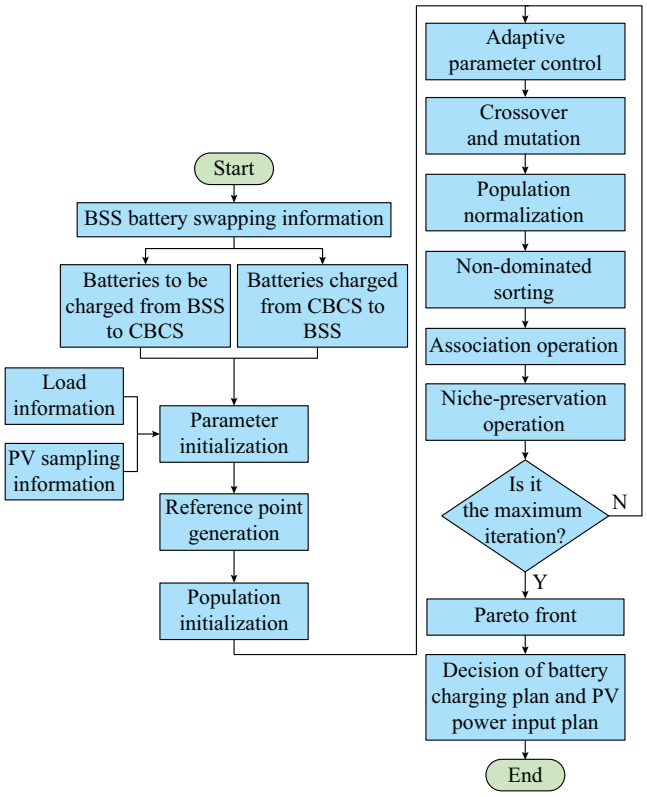

Fig. 7. Flow chart of solving process in operation of CBSCS with PV integration.

Subsequently, we conduct the iterative optimization until the number of iterations reaches the maximum value. Firstly, the rates of crossover and mutation are adaptively controlled. Secondly, we implement the crossover and mutation operation to the parent population, for deriving the offspring population. Thirdly, the parent and offspring populations are mixed together to obtain the combined ones. After that, we normalize the combined population.

Since the optimal individuals need to be selected, we conduct non-dominated sorting to the normalized population to derive several non-domination levels. Afterwards, each population individual is associated with a reference point to obtain a better solution. It is noted that there still exist several vacant slots in the new parent population, and they are filled via updating the niche counts. In the end, the Pareto front and the optimal Pareto solutions are gained. Hence, the operator of CBSCS could use the fuzzy decision-making method [47], in order to obtain the plans of battery charging and PV power input.

VI. Case Study

A. Case Description

The multi-objective optimization scheduling model of CBSCS is processed by parallel computing for enhancing the processing speed, using the Parallel Computing Toolbox of MATLAB [48]. The optimization procedure is on a worksta-

tion with an Intel® Core i7 (2.60 GHz, 64 bit) processor, 16 GB of RAM, and MATLAB R2017b. In this case, CBSCS is connected to a distribution network. In the CBCS, the number of chargers N_{OI} is 1000. Meanwhile, the charging efficiency is set to be 0.9. The dispatching time interval is from 08:00 to 07:00 of the next day, as shown in Fig. 8. CBCS provides charging service to three bus lines, and their operation time intervals are all from 05:30 to 23:00. The average energy consumption per kilometer e_{av} is 1.2 kWh/km. Meanwhile, the peak periods are from 07:00 to 09:00 and 17:00 to 19:00. The mileage per circle and the dispatching interval are 20 km and 6 min, respectively. The average speed in peak and normal periods are 15 km/h and 30 km/h, respectively. In addition, there are 4 batteries in each vehicle, and 30 buses in each line.

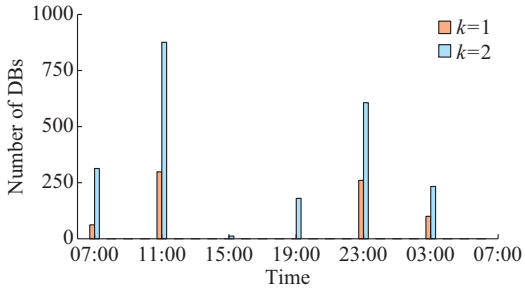

Fig. 8. Number of DBs in CBCS in different time intervals.

Regarding the operation of taxi, we set the total quantity as 1200. There are 1000 taxies whose drivers are shifted every 24 hours and 200 taxies every 12 hours. The capacity of each battery C_{r} is 40 kWh. The lower and upper bounds of SOC are set to be 0.2 and 0.9, respectively. In addition, batteries are divided into two categories and their charging time is set as 1 hour and 2 hours, respectively. For the dispatching time interval ΔT, we set it to be 4 hours.

In addition, PV power is also integrated into CBSCS to satisfy the charging load demand. Concretely speaking, the actual PV power can be obtained by forecasting values and forecasting errors. Meanwhile, the latter is based on the Normal distribution $\mathcal{N}\left(0,\sigma_t^2\right)$, where σ_t is denoted as the SD and set as 8% of the forecasting value at time t. The forecasting values of PV power P_{pre} are set and shown in Fig. 9. Furthermore, K_{L} and K_{H} are set to be 10 and 20 \$/MWh, respectively.

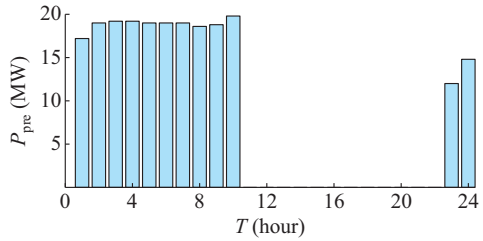

Fig. 9. Forecasting values of 24-hour PV power set.

B. Pareto Front Comparison

In order to better show the effectiveness of modified NSGA-III, we compare it with conventional NSGA-III, NSGA-II and some frequently used heuristic algorithms, i.e., multi-objective particle swarm optimization (MOPSO) [49], multi-objective differential evolution algorithm (MODE) [50], and multi-objective evolutionary algorithm based on decomposition (MOEA/D) [51]. For these six algorithms, their population sizes are all set as 100. Meanwhile, the iteration numbers of these six algorithms are all set to be 6000. For NSGA-II, the distribution indices for crossover and mutation operators are both set to be 20, respectively. In conventional NSGA-III, the rates of crossover and mutation are set as 0.9 and 0.1, respectively, while in the modified NSGA-III, we set the initial rates of crossover and mutation to be 0.95 and 0.83, respectively. In addition, for MOPSO, the personal and global learning coefficients are both set to be 1. Moreover, in the MODE, the amplification and crossover factors F and C_{R} are set to be 0.8 and 0.1, respectively. Meanwhile, in the MOEA/D, the size of neighborhood is set to be 20. What is more, the computation time of our modified NSGA-III is about 1.4 hours. Note that the studied multi-objective optimization scheduling model is based on day-ahead scheduling, i.e., 24 hours, which means that the computation time of our proposed algorithm would be acceptable.

The Pareto fronts obtained from these algorithms are shown in Fig. 10(a). Note that the obtained Pareto fronts are derived from the best ones in 20 independent experiments with respect to each optimization algorithm. It is evident that the modified NSGA-III finds more convergent optimal Pareto solutions, as its Pareto front is under the ones gained by the conventional NSGA-III, NSGA-II, and other heuristic algorithms. For instance, the modified algorithm obtains the least values of TOC and the SD of load, which are ¥39881 and 0.19 MW, respectively. However, such values found by NSGA-II are ¥40926 and 1.52 MW, respectively, which means that it performs much worse than the modified NSGA-III. Also, the points in the Pareto front with respect to NSGA-II are not evenly distributed.

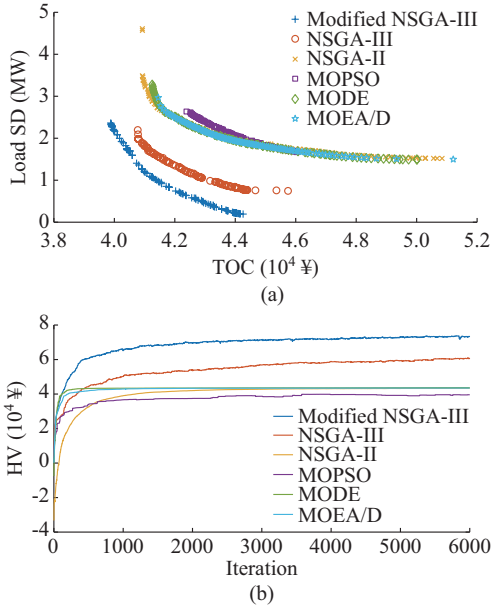

Fig. 10. Comparison of Pareto fronts and hypervolume (HV) with different algorithms. (a) Pareto fronts of TOC and load SD. (b) Values of HV.

In addition, we use detailed metric comparison to show the superiority of the modified NSGA-III, i.e., HV [52], the spacing index, and the mean Euclidian distance (MED) [53]. The index of HV can well evaluate the quality of the Pareto fronts obtained by multi-objective optimization algorithms. It is calculated by the volume covered by the non-dominated solutions, with respect to a reference point in the objective function space. When all objectives are minimized and the values of reference point are chosen as larger ones, the higher value of the HV means the better quality of the obtained Pareto front [52]. The spacing index measures how evenly the points are distributed in the Pareto front, and MED is the averaged Euclidian distance between each point and the selected reference one [53].

In this paper, we set the reference point as (¥60000, 4 MW). The convergence analysis and the metric comparison results are obtained and shown in Fig. 10(b) and Table II, respectively.

TABLE II
METRIC COMPARISON AMONG PARETO FRONTS IN FIG. 10

Algorithm	HV (¥)	Spacing index	MED
Modified NSGA-III	73442	1.5874×10^{3}	1.8108×10^{4}
NSGA-III	60790	1.1166×10^{3}	1.7568×10^{4}
NSGA-II	43351	3.5308×10^{3}	1.5322×10^{4}
MOPSO	39600	7.8240×10^{2}	1.5957×10^{4}
MODE	43723	2.9735×10^{3}	1.5597×10^{4}
MOEA/D	43456	7.8800×10^{1}	1.5521×10^{4}

It could be found that with the iterative process, the values of HV become larger and keeps relatively stable after Pareto solutions are converged. In addition, from Table II, the index of HV with respect to the modified NSGA-III is the largest, i.e., ¥73442, which further verifies that it obtains the best Pareto front, compared with those of other optimization algorithms. Also, it corresponds to the largest MED, which means the Pareto solutions regarding this algorithm are the most convergent. Indeed, it is worth mentioning that the value of spacing index derived by the modified NSGA-III, i.e., 1.5874×10^{3}, is larger than those of conventional NSGA-III, MOPSO, and MOEA/D. However, we could obviously see that the Pareto front of the modified NSGA-III is obviously more convergent.

The reason why the modified NSGA-III performs better than the conventional one is that we adaptively tune the rates of crossover and mutation. The fast non-dominated sorting dominates the time complexity of NSGA-II, i.e., $O(MN^2)$ [47]. In terms of NSGA-III, the non-dominated sorting and associate operation dominate the time complexity of NSGA-III [31]. The non-dominated sorting in NSGA-III requires $O(N^2\lg^{M-2}N)$ for each generation, and the associate operation needs $O(MN^2)$. Therefore, the time complexity of NSGA-III is $\max\{O(N^2\lg^{M-2}N), O(MN^2)\}$. For the modified NSGA-III, we adopt the adaptive parameter control method for tuning the rates of crossover and mutation. In this way, the time complexity of this modification is $O(N)$, which is negligible compared with $\max\{O(N^2\lg^{M-2}N), O(MN^2)\}$. Consequently, the time complexity of the modified NSGA-III is the same as that of the conventional NSGA-III. In this way, it can be seen that the modified algorithm obtains a better Pareto front due to the adaptive tuning of the rates of crossover and mutation, without increasing time complexity compared with NSGA-III.

Therefore, according to the above discussion, it is concluded that the modified NSGA-III can well solve the multi-objective scheduling problem in the proposed CBSCS, and the optimal Pareto solutions could be provided for the decision making of operators.

C. Solution Analysis

The final scheduling solution, i.e., the decision solution could be selected by the fuzzy decision method with equal weights corresponding to the two objectives. In this subsection, we compare the performance of the decision solution with two extreme solutions. Note that the extreme solutions are the optimal solutions for the two individual objectives of TOC and load SD, respectively. Therefore, we denote the decision solution, the extreme solutions of optimal TOC, and optimal load SD as the solutions A, B, and C, respectively.

As shown in Table III, we present the objective values regarding the decision solution and extreme solutions. In addition, the four components of TOC and the electricity load information regarding these solutions in each time interval are shown in Figs. 11-15. Note that the electricity load is the sum of non-charging and charging loads in (18), i.e., $P^t_{\text{load}} = P^t_{\text{local}} + P^t_{\text{c}}$. Besides, Table IV presents load values in each time interval, and the load SDs of solutions A, B, and C can be obtained and presented.

TABLE III
OBJECTIVE VALUES REGARDING DECISION AND EXTREME SOLUTIONS

Solution	C_{L}	R_{H}	C_{R}	C_{S}	TOC (¥)	Load SD (MW)
Solution A	0.4571	0.2708	3.1952	0.7361	41176	1.09
Solution B	0.5064	0.2715	3.1810	0.5723	39881	2.36
Solution C	0.4251	0.2756	3.4608	0.8156	44260	0.19

In Figs. 11-14, we can observe that the operation costs of solution A in the 2nd-5th time intervals and those of solution B in the 1st-6th, 8th and 24th time intervals are obviously less than those of solution C. Moreover, we find that the OC of power shortage and the SCPP usually occur at night, since the PV power is 0 during this time. On the contrary, the OR of PV power surplus mostly occurs in the daytime. Meanwhile, it could be noticed that the OCs of power shortage of solution A in the 1st, 2nd, 20th, and 22nd time intervals and those of solution B in the 1st, 2nd, 6th, 21st, and 22nd time intervals are obviously less than those of C. Furthermore, the ORs of power surplus of Solution B in the 8th time interval are much more than those of solution C. Regarding the SCPPs of solutions A and B, we could observe that they are less in the 3rd-5th, 23rd, and 24th time intervals, compared with the SCPP of solution C.

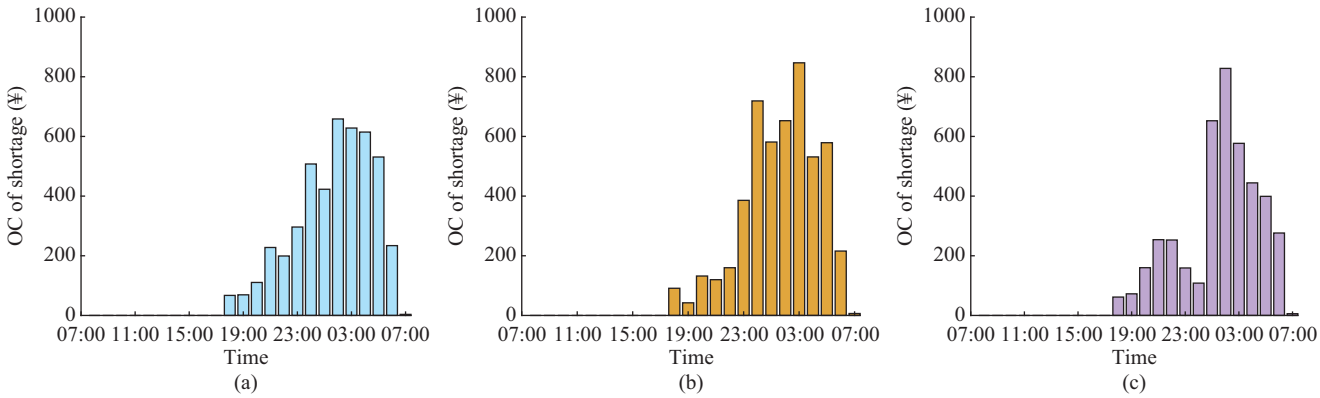

Fig. 11. OCs of shortage with different solutions. (a) Solution A. (b) Solution B. (c) Solution C.

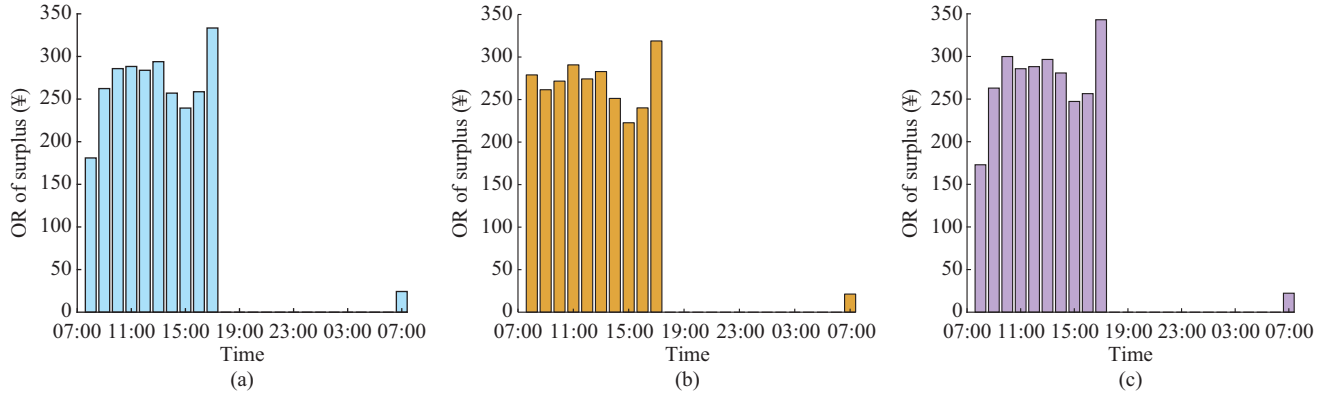

Fig. 12. ORs of surplus with different solutions. (a) Solution A. (b) Solution B. (c) Solution C.

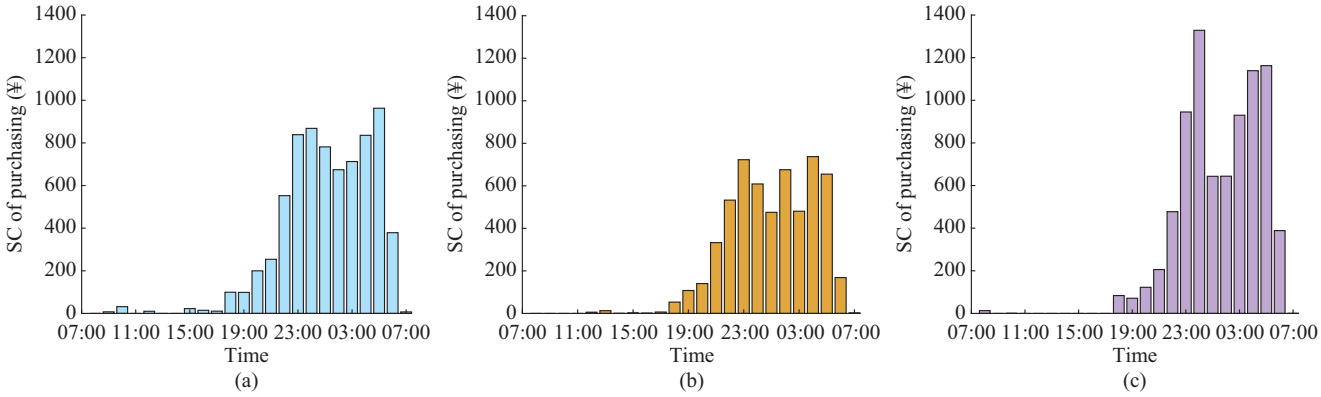

Fig. 13. SCs of purchasing with different solutions. (a) Solution A. (b) Solution B. (c) Solution C.

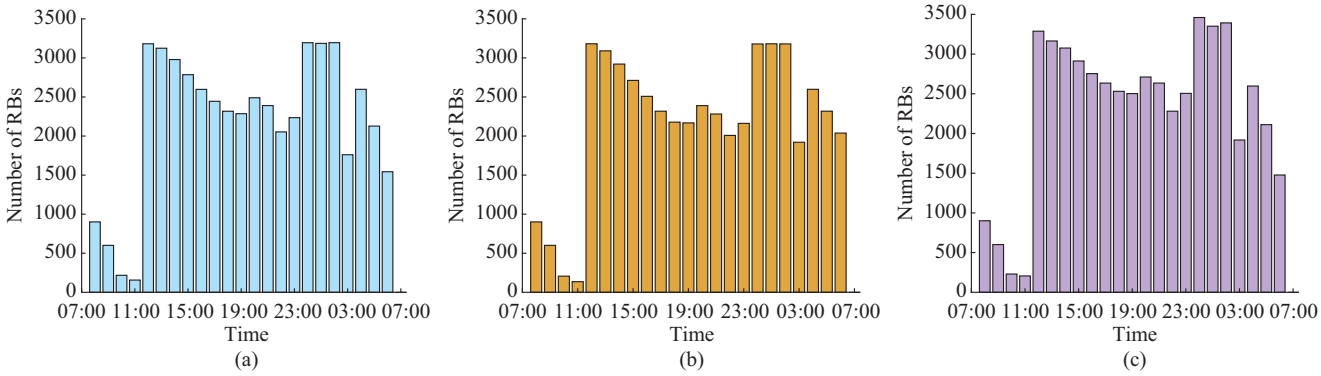

Fig. 14. Number of RBs with different solutions. (a) Solution A. (b) Solution B. (c) Solution C.

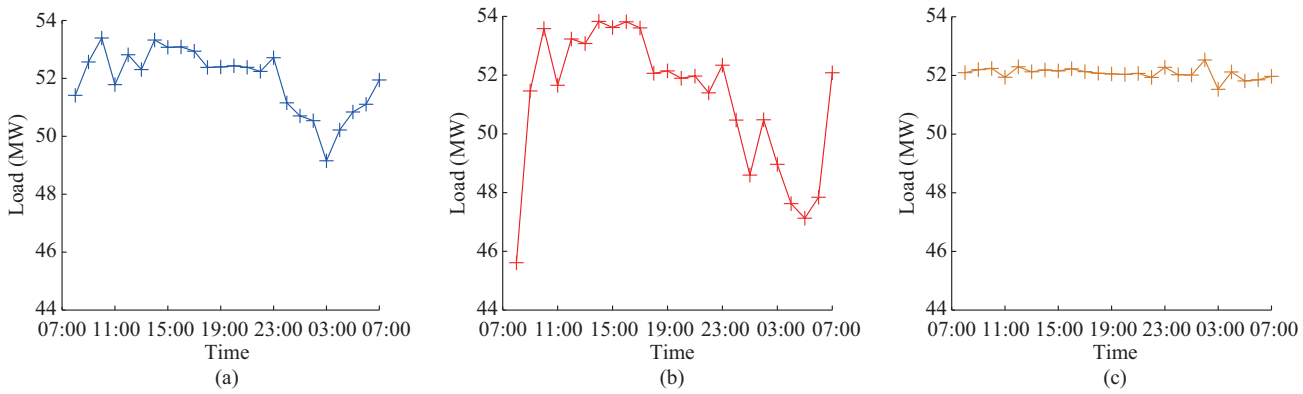

Fig. 15. Load values with different solutions. (a) Solution A. (b) Solution B. (c) Solution C.

TABLE IV
LOAD VALUES WITH DIFFERENT SOLUTIONS IN EACH TIME INTERVAL

Time	P^t_{local} (MW)			Time	P^t_{local} (MW)		
	Solution A	Solution B	Solution C		Solution A	Solution B	Solution C
08:00	51.4	45.6	52.1	20:00	52.4	51.9	52.0
09:00	52.6	51.5	52.2	21:00	52.4	52.0	52.1
10:00	53.4	53.6	52.2	22:00	52.2	51.4	51.9
11:00	51.8	51.7	51.9	23:00	52.7	52.3	52.3
12:00	52.8	53.2	52.3	24:00	51.2	50.5	52.0
13:00	52.3	53.1	52.1	01:00	50.7	48.6	52.0
14:00	53.3	53.8	52.2	02:00	50.5	50.5	52.5
15:00	53.1	53.6	52.2	03:00	49.2	49.0	51.5
16:00	53.1	53.8	52.2	04:00	50.2	47.6	52.1
17:00	52.9	53.6	52.1	05:00	50.8	47.1	51.8
18:00	52.4	52.1	52.1	06:00	51.1	47.8	51.9
10:00	52.4	52.1	52.1	07:00	51.9	52.1	52.0

In addition, it is worth mentioning that the inventory cost of RBs is fixed in the day, since the scheduling of battery charging is for the day-ahead time window. Therefore, we merely need to consider the maximum value of RBs in each time interval. As shown in Fig. 14, we also show the number of RBs with respect to different solutions. It can be noticed that the numbers for solutions A and B are smaller than those of solution C. Accordingly, if the decision makers prefer to minimize the cost, they should choose the solution B, as this solution could obtain the least TOC, i.e., ¥39881. However, the corresponding load SD is as high as 2.36 MW, which is the largest among the mentioned solutions, which means the load fluctuation is not well mitigated for solution B.

D. Uncertainty Analysis

Subsequently, in order to better present the significance of considering the uncertainty of PV power, we conduct comparisons of the optimal Pareto fronts in two cases. Concretely speaking, one is that we obtain the uncertain solution set when $\sigma = 8\%$. The other is that we use $\sigma = 0.01\%$ to obtain the quasi-deterministic solution set. It should be mentioned that we could not set $\sigma = 0$, which would lead to the issue that the OC of PV power shortage and the OR of PV power surplus in (18) are meaningless.

It is also noted that we test the performance of quasi-deterministic solution set, i.e., deriving the values of TOC and load SD with the PV power samples when $\sigma = 8\%$, in order to demonstrate it is necessary to consider the uncertainties in our work. In other words, if the performance of quasi-deterministic solution set is worse in the uncertain environment, we could verify this issue.

Figure 16 shows the two Pareto fronts regarding the uncertain and the quasi-deterministic solution sets, respectively. It is evident that the Pareto front of the uncertain solution set is better. The range of Pareto front regarding quasi-deterministic solution set is [¥40578, ¥46918] and [1.733 MW, 3.04 MW], larger than [¥39881, ¥4.4260] and [0.19 MW, 2.36 MW] for the uncertain solution set. Concretely speaking, the quasi-deterministic solution set could only obtain the optimal TOC as ¥40578, the performance of which is obviously worse than that of the uncertain solution set, i.e., ¥39881. Analogously, the optimal load SD of the uncertain solution set, i.e., 0.19 MW, is also outperformed, compared with that of the quasi-deterministic solution set. Hence, we verify that it is necessary for the dispatchers to consider the uncertainty of PV power, which could help the system adapt the uncertain situation.

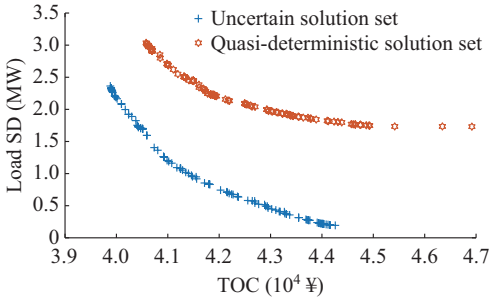

Fig. 16. Pareto fronts of uncertain and quasi-deterministic solution sets.

VII. CONCLUSION

In this paper, we have proposed a multi-objective optimization scheduling model for CBSCS with PV integration. The proposed model has realized the interaction among the battery swapping of users, the battery charging, and the CBSCS. Meanwhile, it simultaneously optimizes the TOC and

the load SD. Then we use a modified NSGA-III to solve the proposed scheduling model. Simulation studies have verified the effectiveness of the proposed model and the modified algorithm. The key conclusions we have found are as follows.

1) It is necessary to consider multi-objective operations of CBSCS by comparing the final decision solution with extreme solutions regarding individual objectives. That is, the balanced consideration of multiple objectives should be taken into account.

2) The multi-objective optimization algorithm of the modified NSGA-III outperforms conventional NSGA-III and NSGA-II, as it can obtain a better Pareto front measured by metric comparisons.

3) We have also found the uncertainty of PV power should be considered in the operation of CBSCS, compared with the quasi-deterministic solution set.

However, there still exist some limitations of our research.

1) The probability distribution we select to model the forecasting error of the PV power is the Normal distribution, and more advanced distribution may be needed for fitting the forecasting error.

2) Our work is based on day-ahead scheduling, and cannot well consider the emergent situation.

In our future work, we will consider degradations of batteries, and investigate their impacts on the operation of the CBSCS with PV integration. Meanwhile, we will adopt more advanced methods to model the forecasting error of PV power. What is more, a real-time scheduling model will be taken into account in future work.

REFERENCES

[1] J. M. Clairand, J. Rodríguez-García, and C. Álvarez-Bel, "Assessment of technical and economic impacts of EV user behavior on EV aggregator smart charging," *Journal of Modern Power Systems and Clean Energy*, vol. 8, no. 2, pp. 356-366, Mar. 2020.

[2] Y. Li, Z. Ni, T. Zhao *et al*., "Supply function game based energy management between electric vehicle charging stations and electricity distribution system considering quality of service," *IEEE Transactions on Industry Applications*, vol. 56, no. 5, pp. 5932-5943, Apr. 2020.

[3] Y. Li, Z. Ni, T. Zhao *et al*., "Coordinated scheduling for improving uncertain wind power adsorption in electric vehicles-wind integrated power systems by multiobjective optimization approach," *IEEE Transactions on Industry Applications*, vol. 56, no. 3, pp. 2238-2250, Feb. 2020.

[4] International Energy Agency. (2016, May). Global EV outlook 2016. [Online]. Available: https://www.iea.org/reports/global-ev-outlook-2016

[5] H. Mak, Y. Rong, and Z. Shen, "Infrastructure planning for electric vehicles with battery swapping," *Management Science*, vol. 59, no. 7, pp. 1557-1575, Jul. 2013.

[6] Q. Kang, J. Wang, M. Zhou *et al.*, "Centralized charging strategy and scheduling algorithm for electric vehicles under a battery swapping scenario," *IEEE Transactions on Intelligent Transportation Systems*, vol. 17, no. 3, pp. 659-669, Mar. 2016.

[7] M. Sarker, H. Pandzic, and M. O. Vazquez, "Optimal operation and services scheduling for an electric vehicle battery swapping station," *IEEE Transactions on Power Systems*, vol. 30, no. 2, pp. 901-910, Jul. 2014.

[8] R. Rao, X. Zhang, J. Xie *et al.*, "Optimizing electric vehicle users' charging behavior in battery swapping mode," *Applied Energy*, vol. 155, no. 1, pp. 547-559, Oct. 2015.

[9] Y. Li, Z. Yang, G. Li *et al.*, "Optimal scheduling of isolated microgrid with an electric vehicle battery swapping station in multi-stakeholder scenarios: a bi-level programming approach via real-time pricing," *Applied Energy*, vol. 232, pp. 54-68, Dec. 2018.

[10] W. Li, X. Tan, B. Sun *et al.*, "Optimal power dispatch of a centralized electric vehicle battery charging station with renewables," *IET Communications*, vol. 12, no. 5, pp. 579-585, Mar. 2018.

[11] S. Wang, L. Lu, X. Han *et al.*, "Virtual-battery based droop control and energy storage system size optimization of a DC microgrid for electric vehicle fast charging station," *Applied Energy*, vol. 259, Feb. 2020.

[12] X. Dong, Y. Mu, X. Xu *et al.*, "A charging pricing strategy of electric vehicle fast charging stations for the voltage control of electricity distribution networks," *Applied Energy*, vol. 225, pp. 857-868, Sept. 2018.

[13] F. Wu and R. Sioshansi, "A two-stage stochastic optimization model for scheduling electric vehicle charging loads to relieve distribution-system constraints," *Transportation Research Part B: Methodological*, vol. 102, pp. 55-82, Aug. 2017.

[14] X. Tan, G. Qu, B. Sun *et al.*, "Optimal scheduling of battery charging station serving electric vehicles based on battery swapping," *IEEE Transactions on Smart Grid*, vol. 10, no. 2, pp. 1372-1384, Oct. 2017.

[15] T. Raviv, "The battery switching station scheduling problem," *Operations Research Letters*, vol. 40, no. 6, pp. 546-550, Nov. 2012.

[16] X, Zhang and G. Wang, "Optimal dispatch of electric vehicle batteries between battery swapping stations and charging stations," in *Proceedings of 2016 IEEE PES General Meeting*, Boston, USA, Jul. 2016, pp. 1-5.

[17] M. Ban, J. Yu, M. Shahidehpour *et al.*, "Electric vehicle battery swapping-charging system in power generation scheduling for managing ambient air quality and human health conditions," *IEEE Transactions on Smart Grid*, vol. 10, no. 6, pp. 6812-6825, Nov. 2019.

[18] A. Ul-Haq, C. Cecati, and E. Ammar, "Modeling of a photovoltaic-powered electric vehicle charging station with vehicle-to-grid implementation," *Energies*, vol. 10, no. 1, pp. 1-20, Dec. 2016.

[19] Q. Chen, N. Liu, C. Hu *et al.*, "Autonomous energy management strategy for solid-state transformer to integrate PV-assisted EV charging station participating in ancillary service," *IEEE Transactions on Industrial Informatics*, vol. 13, no. 1, pp. 258-269, Feb. 2017.

[20] K. Seddig, P. Jochem, and W. Fichtner, "Two-stage stochastic optimization for cost-minimal charging of electric vehicles at public charging stations with photovoltaics," *Applied Energy*, vol. 242, pp. 769-781, May 2019.

[21] W. Tushar, C. Yuen, S. Huang *et al.*, "Cost minimization of charging stations with photovoltaics: an approach with EV classification," *IEEE Transactions on Intelligent Transportation Systems*, vol. 17, no. 1, pp. 156-169, Jan. 2016.

[22] S. Wu, Q. Xu, Q. Li *et al.*, "An optimal charging strategy for PV-based battery swapping stations in a DC distribution system," *International Journal of Photoenergy*, vol. 2017, no. 8, pp. 1-11, Apr. 2017.

[23] Y. Cheng and C. Zhang. "Configuration and operation combined optimization for EV battery swapping station considering PV consumption bundling," *Protection and Control of Modern Power Systems*, vol. 2, no. 1, pp. 1-18, Jul. 2017.

[24] H. H. Eldeeb, S. Faddel, and O. A. Mohammed, "Multi-objective optimization technique for the operation of grid tied PV powered EV charging station," *Electric Power Systems Research*, vol. 164, pp. 201-211, Nov. 2018.

[25] W. Yu, S. Liu, Q. Chen *et al.*, "Multi-objective optimization scheduling for PV microgrid considering electric vehicle charging and demand response," *Proceedings of the CSU-EPSA*, vol. 30, no. 1, pp. 88-97, Jan. 2018.

[26] Z. Chen, X. Xiao, X. Lu *et al.*, "Multi-objective optimization for capacity configuration of PV-based electric vehicle charging stations," *Transactions of China Electrotechnical Society*, vol. 28, no. 6, pp. 238-248, Jun. 2013.

[27] M. F. El-Naggar and A. A. A. Elgammal, "Multi-objective optimal predictive energy management control of grid-connected residential wind-PV-FC-battery powered charging station for plug-in electric vehicle," *Journal of Electrical Engineering and Technology*, vol. 13, no. 2, pp. 742-751, Mar. 2018.

[28] N. Liu, Z. Chen, J. Liu *et al.*, "Multi-objective optimization for component capacity of the photovoltaic-based battery switch stations: towards benefits of economy and environment," *Energy*, vol. 64, pp. 779-792, Jan. 2014.

[29] G. Zhao, X. Huang, and H. Qiang, "Coordinated control of PV generation and EVs charging based on improved DECell algorithm," *International Journal of Photoenergy*, vol. 2015, no. 4, pp. 1-13, May 2015.

[30] S. R. Canan, B. Shantanu, and L. W. Van, "Closed-loop supply chain models with product remanufacturing," *Management Science*, vol. 50, no. 2, pp. 239-252, Feb. 2004.

[31] K. Deb and H. Jain, "An evolutionary many-objective optimization algorithm using reference-point based non-dominated sorting approach, Part I: solving problems with box constraints," *IEEE Transactions on*

Evolutionary Computation, vol. 18, no.4, pp. 577-601, Aug. 2014.
[32] L. Shi, C. Wang, L. Yao *et al.*, "Optimal power flow solution incorporating wind power," *IEEE Systems Journal*, vol. 6, no. 2, pp. 233-241, Jun. 2012.
[33] J. R. Stock, "Reverse logistics," in *Oak Brook*: *Council of Logistics Management*, Chicago: Oak Brook, 1992.
[34] H. Krikke, C. P. Pappis, G. T. Tsoulfas *et al.*, "Extended design principles for closed loop supply chains: optimizing economic, logistic and environmental performance," *Economics and Mathematical Systems*, vol. 519, pp. 45-47, Jan. 2001.
[35] F. J. M. Salzborn, "Optimum bus scheduling," *Transportation Science*, vol. 6, no. 2, pp. 137-148, May 1972.
[36] X. Wang, L. Sun, F. Wen *et al.*, "Modeling charging demands of various types of electric vehicles in an actual distribution system," in *Proceedings of IEEE PES Asia-Pacific Power and Energy Engineering*, Brisbane, Australia, Nov. 2015, pp. 1-5.
[37] V. B. Vu, D. H. Tran, and W. Choi, "Implementation of the constant current and constant voltage charge of inductive power transfer systems with the double-sided LCC compensation topology for electric vehicle battery charge applications," *IEEE Transactions on Power Electronics*, vol. 33, no. 9, pp. 7398-7410, Sept. 2018.
[38] Z. Luo, Z. Hu, Y. Song *et al.*, "Optimal coordination of plug-in electric vehicles in power grids with cost-benefit analysis—Part I: enabling techniques," *IEEE Transactions on Power Systems*, vol. 28, no. 4, pp. 3546-3555, Nov. 2013.
[39] Z. Hu, K. Zhan, H. Zhang *et al.*, "Pricing mechanisms design for guiding electric vehicle charging to fill load valley," *Applied Energy*, vol. 178, pp. 155-163, Sept. 2016.
[40] C. S. Ioakimidis, D. Thomas, P. Rycerski *et al.*, "Peak shaving and valley filling of power consumption profile in non-residential buildings using an electric vehicle parking lot," *Energy*, vol. 148, pp. 148-158, Apr. 2018.
[41] K. Zhang, L. Xu, M. Ouyang *et al.*, "Optimal decentralized valley-filling charging strategy for electric vehicles," *Energy Conversion and Management*, vol. 78, pp. 537-550, Feb. 2014.
[42] S. Eric, M. H. Mohammad, S. D. James *et al.*, "Coordinated charging of plug-in hybrid electric vehicles to minimize distribution system losses," *IEEE Transactions on Smart Grid*, vol. 2, no. 1, pp. 198-205, Apr. 2011.
[43] K. Deb, A. Pratap, S. Agarwal *et al.*, "A fast and elitist multi-objective genetic algorithm: NSGA-II," *IEEE Transactions on Evolutionary Computation*, vol. 6, no. 2, pp. 182-197, Jan. 2002.
[44] M. Srinivas and L. M. Patnaik, "Adaptive probabilities of crossover and mutation in genetic algorithms," *IEEE Transactions on Systems Man and Cybernetics*, vol. 24, no. 4, pp. 656-667, Apr. 1994.
[45] I. Das and J. Dennis, "Normal-boundary intersection: a new method for generating the Pareto surface in nonlinear multicriteria optimization problems," *SIAM Journal of Optimization*, vol. 8, no. 3, pp. 631-657, Jul. 2000.
[46] Y. Shi and R. C. Eberhart, "Empirical study of particle swarm optimization," in *Proceedings of the 1999 Congress on Evolutionary Computation*, Washington DC, USA, Jul. 1999, pp. 1945-1950.
[47] T. Niknam, R. Azizipanah-Abarghooee, and M. R. Narimani, "An efficient scenario-based stochastic programming framework for multi-objective optimal micro-grid operation," *Applied Energy*, vol. 99, pp. 455-470, Nov. 2012.
[48] MathWorks. (2019, May). GPU computing. [Online]. Available: https://ch.mathworks.com/solutions/gpu-computing.html
[49] C. A. C. Coello, G. T. Pulido, and M. S. Lechuga, "Handling multiple objectives with particle swarm optimization," *IEEE Transactions on Evolutionary Computation*, vol. 8, no. 3, pp. 256-279, Jul. 2004.
[50] M. Ali, P. Siarry, and M. Pant, "An efficient differential evolution based algorithm for solving multi-objective optimization problems," *European Journal of Operational Research*, vol. 217, no. 2, pp. 404-416, Mar. 2012.
[51] Q. Zhang and H. Li, "MOEA/D: a multiobjective evolutionary algorithm based on decomposition," *IEEE Transactions on Evolutionary Computation*, vol. 11, no. 6, pp. 712-731, Jan. 2008.
[52] K. Bringmann and T. Friedrich, "Approximation quality of the hypervolume indicator," *Artificial Intelligence*, vol. 195, pp. 265-290, Feb. 2013.
[53] M. A. C. Silva, C. E. Klein, V. C. Mariani *et al.*, "Multiobjective scatter search approach with new combination scheme applied to solve environmental/economic dispatch problem," *Energy*, vol. 53, pp. 14-21, May 2013.

Yuanzheng Li received the M.S. degree from Huazhong University of Science and Technology, Wuhan, China, in 2011, and the Ph.D. degree in electrical engineering from South China University of Technology, Guangzhou, China, in 2015. His current research interests include optimal power system dispatch and decision making.

Yihan Cai received the B.S. degree from Huazhong University of Science and Technology, Wuhan, China, in 2019. His current research interests include optimal power system dispatch and decision making.

Tianyang Zhao received the B.Sc. and M.Sc. degrees in automation of electric power systems from North China Electric Power University, Beijing, China, in 2011 and 2013, respectively. Currently, he is a Research Fellow in Nanyang Technological University, Singapore, Singapore. His current research interests include electricity market and game theory.

Yun Liu received the B.Eng. and the Ph.D. degrees from the College of Electrical Engineering, Zhejiang University, Hangzhou, China, in 2011 and 2016, respectively. From 2016 to 2017, he was with the Energy Research Institute, Nanyang Technological University, Singapore, Singapore, as a Research Fellow. He is currently an Assistant Professor with the College of Mechatronics and Control Engineering, Shenzhen University, Shenzhen, China. His research interests include power system stability analysis, photovoltaic generation, microgrid, and distributed control and optimization.

Jian Wang received the Ph.D. degree in automation and system engineering from Huazhong University of Science and Technology, Wuhan, China, in 2009. He is currently an Associate Professor in the same university. His current research interests include optimization and simulation of logistics and supply chain system.

Lei Wu received the B.S. degree in electrical engineering and the M.S. degree in systems engineering from Xi'an Jiaotong University, Xi'an, China, in 2001 and 2004, respectively, and the Ph.D. degree in electrical engineering from the Illinois Institute of Technology, Chicago, USA, in 2008. He was a Professor with the Electrical and Computer Engineering Department, Clarkson University, Potsdam, USA, till 2018. Currently, he is an Associate Professor with the Electrical and Computer Engineering Department, Stevens Institute of Technology, Hoboken, USA. His research interests include power system operation and planning, energy economics, and community resilience microgrid.

Yong Zhao received the Ph.D. degree in automation and system engineering from Huazhong University of Science and Technology, Wuhan, China, in 1996. He is currently a Professor in the same university. His current research interests include decision making theory, system analysis, and integration.